Carpathian Journal of Earth and Environmental Sciences, May 2015, Vol. 10, No. 2, p. 175 - 188

FOREST ENVIRONMENT MONITORING IN THE OCNELE MARI AREA USING SYNTHETIC APERTURE RADAR DATA

Violeta POENARU[1,2], Alexandru BADEA[1] & Sorin CIMPEANU[2]

[1]*Romanian Space Agency, Space Applications Department, 010362, Bucharest, Sector 1, 21-25 Mendeleev, Romania, violeta.poenaru@rosa.ro, alexandru.badea@rosa.ro*

[2]*University of Agronomic Science and Veterinary Medicine, 011464, Bucharest, Bulevardul MARASTI nr. 59, Romania, mscimpeanu@yahoo.fr*

Abstract: Monitoring of the environmental impact of mines is important for the evaluation of the land and vegetation cover degradation, water pollution, destruction and disturbance of ecosystems and habitats. Ocnele Mari salt mine area is one of the disused mine affected by degradation phenomena with direct impact of environment and human health. The paper investigates Synthetic Aperture Radar techniques capabilities to monitor forest environment in the Ocnele Mari salt mining area. The presence of vegetation in the area monitored through interferometric techniques leads to the decrease in correlation between data acquisitions which translate into lower coherence values. Persistent scatterer interferometry analysis is performed to estimate the phase of stable natural reflectors for land deformation assessment. The PSInSAR results confirm the leveling measurements: a decreasing trend in subsidence rate (about few millimeter/year) is observed. The coherence change detection approaches reveals that land changes can be observed in urban and non-vegetated areas while the amplitude change detection is less sensitive to subtle changes and provides valuable information about vegetation stage and moisture content. Polarimetric SAR interferometry analysis is performed to estimate forest height. The extracted heights from RADARSAT-2 data images vary between 18 and 60 m whereby heights above 50 m occur more frequently in far range.

Keywords: Vegetation land cover, land degradation, forest height estimation, PSInSAR, PolInSAR, Ocnele Mari

1. INTRODUCTION

The environment monitoring, anytime and in any weather conditions, is possible by using the Synthetic Aperture Radar (SAR) techniques. For obtaining a high resolution, a very large aperture is synthetised over the flight path of a satellite platform whose sensor emits an electromagnetic radiation in the microwave frequencies domain. The SAR sensors, that could operate in P, L, S, C, K or Ku band, are equipped with a transmitter highlighting the area of interest and a receiver for recording the electromagnetic backscattered radiation.

Since June 1978, when the first satellite carrying a synthetic aperture radar was been launched, many SAR missions were focused on Earth Observation studies for improving environmental monitoring, marine surveillance, ice monitoring, disaster management, resource management and mapping. The progress was possible by developing new techniques and methods allowing the estimation and mapping at a considerable spatial resolution in synergy with the size of the heterogeneities within fields. Radar signal processing and analysis (Cumming & Wong, 2005), radar polarimetry by PolSAR and PolinSAR (Claude & Pottin, 1996) techniques or radar based on interferometry such as InSAR (Zebker & Goldstein, 1986), DInSAR (differential interferometry) and PSInSAR (persistent scatter interferometry) techniques could be successfully applied for environmental monitoring and mapping.

The objective of this paper is the evaluation of the SAR techniques with emphasis on temporal requirements and associated accuracy of outputs such as vegetation coverage and/or land degradation estimation in the Ocnele Mari salt mining area.

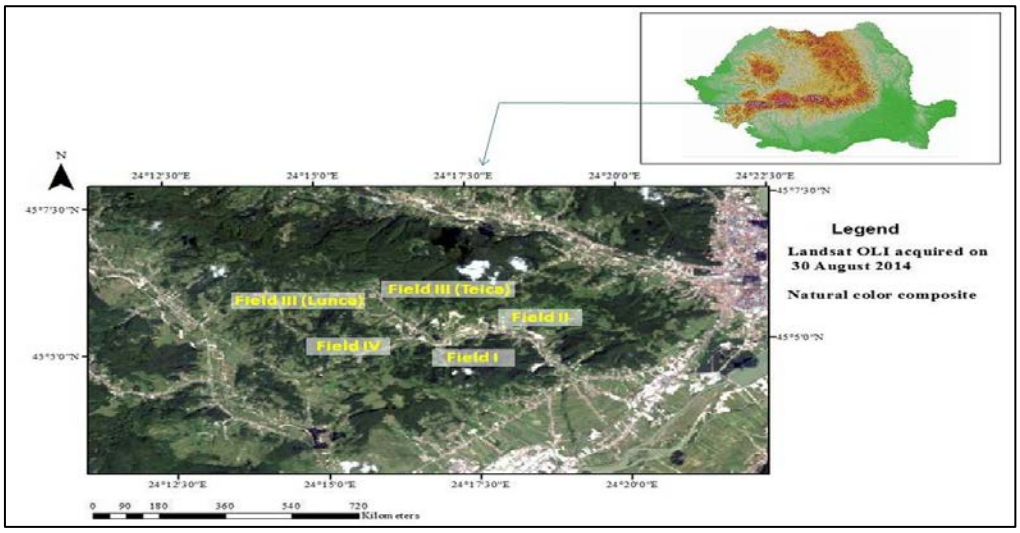

Figure 1. Map of the Ocnele Mari salt mining area

The test site, located in a hilly region surrounded by vegetation coverage (Fig. 1), is affected by land deformation (subsidence and landslides) (Bălteanu, 2000; Bălteanu et al., 2006) as well as vegetation degradation (Poenaru et al., 2011).

The Ocnele Mari salt mines area is affected by scattering problems: due to layover effects, the SAR data could contain corrupted height information, which can be adjusted by a DEM. A double bounce scattering mechanism enables the land deformation estimation while volume scattering mechanism introduces a noisy phase signal that is not included in the deformation map. The state of the problem differs in the polarimetric radar data: a double bounce mechanism is present in the single-polar channel and is obtaining by the scattering between the tree trunks and the ground level, while volume scattering is observing in all channels and represents the backscattering contribution from the randomly oriented needles in the crown (Pottier et al., 2004). The differences in height between these scattering mechanisms allow estimating the height of the forest. In this context, based on TerraSAR-X, RADARSAT-2 and Sentinel-1 data and applying different SAR techniques, the environmental conditions from Ocnele Mari are investigated and mapped.

2. METHODS

2.1. SAR interferometry (InSAR)

SAR interferometry is a technique that directly measures the phase changes between two-phase measurements of the same ground pixel of the Earth surface. As SAR is a coherent image system, InSAR employ two complex valued images to derive additional information about a scene by exploiting differences in the amplitude and phase for the interferogram generation. Therefore, the interferometric coherence, expressed as correlation coefficient (eq. 1), reflects the degree of similarity between the image pair: 0 magnitude value for a total decorrelation (no phase information) and 1 for no phase noise.

$$\hat{\gamma} = \frac{\Sigma_{r_n} \Sigma_{x_m} v_1 v_2^* e^{-j\phi(r_n, x_m)}}{\sqrt{\Sigma \Sigma |v_1|^2 \Sigma \Sigma |v_2|^2}} \qquad (1)$$

The coherence also depends on the radar signal interaction with the ground surface, which involves scattering and absorption mechanisms. A loss of coherence can be caused by noise and temporal changes of the scattering properties of the target, volumetric effects (volume scattering and large baselines) and this because of the effective path length variations over the scene, which can be attributed to topographic, atmospheric, or deformation gradients (eq. 2) (Ferretti et al., 2007).

$$\gamma = \gamma_T * \gamma_G * \gamma_V * \gamma_P \qquad (2)$$

Where: γ_T- temporal decorrelation;
γ_G - geometric error;
γ_V - volumetric effects;
γ_P - processing errors.

Additionally, the systematic phase variation is affecting the coherence estimation window too.

An interferogram contains the interferometric phase fringes from SAR sensor geometry, together with those from atmospheric contribution, topography and displacement of the surface. The fringe number from InSAR geometry is strongly dependent on the baseline perpendicular component. This is a criterion which is applied to SAR data acquisition: small perpendicular baseline to optimise the coregistration process and to reduce the topography phase contribution.

InSAR processing procedures for coherence

map generation are described below. First, the slave SAR complex data is resampled at the master dimension. The SAR images are co-registered for the formation of the interferogram image pair. Layover and shadowing effects may result because some misalignments at the image pair coregistration. The geometric phase of the system is removing by using the Earth flattening procedure. By applying an external digital elevation model for subtracting the topographic phase, the coherence is calculated. The phase unwrapping, as process used to reconstruct the original phase, constitutes an important step of the InSAR processing. The mountain and hilly areas introduce the layover effects that appear as discontinuity in the interferogram which is not caused by noise. Goldstein et al., (1988) proposed a phase unwrapping method based on branch-cut algorithm by connecting nearest residues and unwrapping pixel-by-pixel without crossing the branch cuts. Finally, the phase deformation in radar look-direction can be estimated (eq.3):

$$\phi = \phi_d = \frac{4\pi}{\lambda} \mathrm{d} \qquad (3)$$

where *d* is relative scatterer displacement projected in the slant range direction.

The applications of the repeat pass SAR interferometry are: (i) topographic mapping with an accuracy of 10 – 50m; (ii) deformation mapping with mm – cm accuracy; (iii) thematic mapping based on coherence or amplitude change detection; and (iv) atmospheric delay mapping.

In the case of the mining activities, the land subsidence estimation depends on the deformation gradient, vegetation coverage, land use and atmospheric signal presence in interferogram. Therefore, for the Ocnele Mari salt mining area where the deformation rate is quite stable at milimeter/ year, the systematic analysis of many very high resolution images to better characterize the signal and noise is required (Mocuta et al., 2010).

Since the mean backscattered power and complex correlation coefficient measure different properties of a scene, coherent (CCD) and incoherent change statistics is applied for thematic changes mapping.

Coherent change detection method uses statistics to identify changes in amplitude and phase that allow detecting very subtle scene changes in the sub-resolution cell scattering structure (Preiss et al., 2006). Also, it exploits the sensitivity of the SAR image speckle pattern and associate image phase to the nature and structure of the scene scattering mechanism. Land deformation and vegetation phonological stages induce measurable changes in speckle pattern and pixel size which lead to a reduction of the cross correlation coefficient and coherence of the image pair. The challenge is to separate as much possible the changed and unchanged pixels using small window size, without multilooking. While change detection based on coherence maps can offer an effective and sensitive indication of the modified areas undergoing subtle ground changes between two subsequent SAR images, its applicability is limited by vegetation cover and topography (Ocnele Mari case).

Incoherent change detection identifies changes in the underlying mean backscatter power of a scene. Based on digital techniques proposed by Singh (1989), many studies (Jiang et al., 2007; Xiong et al., 2012; Aghababaee et al., 2013) focused on improving the change detection methods to increase precision accuracy. It is found that this technique, applied to a multi-temporal SAR dataset, can monitor modifications that occur over an area by tracking temporal variations of the backscattering coefficient of the target surfaces.

2.2 Persistent Scatterer Interferometry

Persistent scatterer interferometry (PSInSAR) is a powerful tool with capability to detect milimeter land deformation (Ferretti et al., 2000; Ferretti et al., 2001). This technique is based on existence of persistent scatterers (PS) which are dense in urban area and may be sparse in natural landscape.

There are three methods to estimate PS candidates representing different approaches. First method estimates deformations for each PS pixels based mainly on their phase variation in time in order to assess and remove nuisance terms (DePSI method developed by Delft University). A second method uses both amplitude and phase analysis to determine the PS probability for individual pixels using correlation of their phase in space (StaMPS). In contrast to DePSI, this method produces a time series of deformation with no prior assumptions about the temporal nature of deformation. By applying a higher threshold value (Hooper et al., 2007) a number of pixels is selected as initial PS candidates. If the pixels persist only in a subset of generated interferograms being also dominated by scatterers in adjacent PS, then they will be rejected. Statistically, the pixels with higher coherence are more likely to be PS. Through multiple iterations the pixels with low coherence are rejected and the patch means are computed using only the remaining candidates. The third method consists in the identification of the PS using thresholds or amplitude dispersion index modelling PSInSAR

time series without phase unwrapping (Zhang et al., 2011). This method works well in areas with linear or nonlinear ground deformation.

It should be noted that all deformation maps must be interpreted in a relative sense because no absolute deformation can be derived from PSInSAR measurements. As the PS measurements are relative to a reference point, the precision of the estimate is high, but the accuracy of PS localisation is relatively poor due to orbit uncertainty, instrumental and propagation delay and scattering centre uncertainty.

2.3 Polarimetric SAR Interferometry

The polarimetric SAR interferometry combines interferometric and polarimetric SAR imaging techniques and provides the ability to use information of different polarization channels to investigate the object structure and perpendicular layers of the scatterer. A conventional interferometric system operates with a fixed polarization at a single frequency and is not able to provide enough information necessary to describe natural scattering processes. Polarimetric systems estimate the location of the effective scattering phase centres which depends on wavelength, polarization and physical and geometrical properties of the scatterer.

Some authors focused on the analysis of scattering mechanism based on target decomposition to classify and characterise the natural surfaces such as vegetation and surface parameters retrieval (Cloude & Papathanassiou, 2002; Lee et al., 2006; Licciardi et al., 2012; Wang et al., 2013). These studies were carried out over relatively flat areas. In the hilly and mountain areas, scatterer signal is strongly affected by the variations of the local incidence angle and the local orientation angle. So, the slope correction is necessary to eliminate the impact of the topography in forest parameters extraction. Furthermore, the coherence phase optimization is necessary for improving the forest height retrieval. Lavalle et al., (2007) proposes several optimization algorithms to extent the coherence region in synergy with the vegetation height increasing. Luo et al., (2010) included non-volume scattering decorrelation factor and applied an inversion algorithm based on coherence amplitude and phase information alone for improving the performance of the inversion method. Fomena (Fomena & Cloude, 2005) suggests using the numerical radius method in the case where the polarimetric properties of the scene are unchanged during the two acquisitions.

Bamler & Hartl, (1998) demonstrated that, after calibrating, the system induces decorrelation contributions and compensation of spectral decorrelation in azimuth and range. In fact, the estimated coherence is decomposed into three decorrelation terms:

$$\tilde{\gamma} = \tilde{\gamma}_{temp}\ \gamma_{SNR}\ \tilde{\gamma}_{vol} \qquad (4)$$

Ignoring the thermal noise and temporal decorrelation, the coherence is analysed function of volume scattering, which allows investigating the vertical structure of forest. A random volume (RV) model assumes that the density of scatterer does not depend on scatterer orientation and the vegetation layer is horizontal so that the vegetation parameters (vegetation height, altitude of the top of the vegetation layer and extinction coefficient) are estimated with an increasing accuracy (Treuhaft & Siqueira, 2000). If the volume is oriented (OV model), incident waves propagate along polarizations determinated by the eigenvectors of the average forward scattering matrix. Each eigenpolarisation is characterized by its own complex wave numbers describing refraction and attenuation (extinction). The vertical distribution of scatterers changes with polarization so that interferometric volume coherence becomes a function of polarization. Optimal interferometric coherence is obtained when eigenpolarisations are orthogonal (H and V polarisations) that correspond to the maximum/ minimum values of the extinction coefficients. These considerations are theoretical because, in a realistic scenario, the interactions between vegetation layer and ground are taken into account. There are two cases: random volume over ground (RVoG) which assumes the propagation through the volume as independent of polarization and orientated volume over ground (OVoG) in which the propagation through the volume changes with polarization. In the RVoG model, the coherence optimization is based on the variation of the ground to volume amplitude ratio, whilst the OVoG model involves the extinction coefficient and the ground to volume amplitude ratio in coherence optimization.

Interpreting the vertical forest dimension as a two layer medium and applying RVoG model, the volume decorrelation is obtained as a function of forest height extinction, volume and ground scattering (eq. 5).

$$\tilde{\gamma}_{vol} = \exp(ik_z z_0)\frac{\tilde{\gamma}_{v0} + m}{1+m} \qquad (5)$$

where z_0 is related to the ground topography, k_z is the vertical wavenumber of the interferometer depending on the imaging geometry ($k_z = \frac{4\pi\Delta\theta}{\lambda\theta_0}$) and m is the effective ground-to-volume amplitude

ratio accounting for the attenuation through the volume$m = m_G/(m_V I_0)$.

$\tilde{\gamma}_{v0}$ Does the vegetation layer given by (Cloude & Papathanassiou, 1998) cause the volume decorrelation:

$$\tilde{\gamma}_{v0} = \exp(ik_z z_0) \frac{\int_0^{h_v} \exp(ik_z z')exp(\frac{2\sigma z'}{cos\theta_0})dz'}{\int_0^{h_v} \exp(\frac{2\sigma z'}{cos\theta_0})dz'} \quad (6)$$

Since polarimetric waves are sensitive to different scattering contributions, PolInSAR technique allows computing these parameters and inverts forest height.

The C-band interferometric phase in vegetated areas represents scattering somewhere inside the vegetation canopy so that forest height could be overestimated in a hilly / mountainous area. Lu et al., (2013) (lower frequency, L-band) developed a sloped random volume over ground model introducing the dependence of PolInSAR coherence on local range terrain slope.

Cloude & Papathanassiou, (2003) developed a three stage inversion process in order to: 1) calculate a maximum coherence separation with a sinc function; 2) determine volume dominated coherence from knowing topography (zero surface component); and 3) invert complex coherence using a coherent scattering model. The inclusion of the phase information provides a deeper understanding of the interaction of the radar wave with forest structure and eliminates the ground-bias in the volume decorrelation. On the other hand, the inversion methodology is more complex than the sinc-inversion and must minimize possible error sources.

3. RESULTS AND DISSCUSION

3.1. Experiment design

The test site considered in this paper is rather complex as it represents continuous alteration of land use/ land cover classes (i.e. deciduous, transition areas with shrubs, natural grasslands, orchards, agricultural fields, urban areas, mines and saline). Levelling measurements performed on the 68 probes, uniformly distributed in the salt mine perimeter, reveal slow subsidence as well as the rapid mining subsidence caused by water inflow into the caverns. Moreover, science the selected area includes an irregular topography; it represents a challenging test case for SAR image analysis.

A set of twenty VHR TerraSAR-X complex SAR images (1 m ground range resolution), acquired between August 2010 and August 2011, a set of four RADARSAT-2 dual polarized complex SAR images and a set of two Sentinel-1 dual polarized SAR images were used for investigation. For processing and validation purposes, a Digital Elevation Model (derived from HRS SPOT data) and a Thematic Mapper Image (acquired by Landsat 8 OLI satellite) were used. An area of 5 X 10 km was selected for the study.

3.2 Results for multi-temporal analysis

The multi-temporal SAR data analysis exploits information carried by changes in backscatter coefficient that are relevant in environmental monitoring. Therefore, we investigated multitemporal behaviour of land use/ land cover classes during one-year time span by applying coherent and incoherent change detection techniques.

Three pairs of TSX data (Table 1) have been processed to generate coherence images. SLC images were corregistrated within 1/32 of a pixel that is accurate enough for most InSAR techniques. This scheme gives shortest baseline between three images that minimize any possible registration error. The InSAR processing steps described in the section 2.1 were performed on the image pairs. A relatively small window with 20 pixels only in azimuth direction satisfied both requirements of high contrast coherence image and high spatial resolution in a hilly region. Figure 2 shows an RGB false color composite of coherence. First and third inferterometric pairs show comparable coherence values with an average range between 0.4-0.6 and standard deviation by +/- 0.1. The second image pair has a slightly higher average coherence and a significantly higher standard deviation. A pixel by pixel analysis of an area will not be successful in determining land degradation in a vegetated area even in a dry winter season. In this case we concluded that the coherence change detection can be used to identify man-made structures. Figure 3 shows an RGB false colour composite of coherence and intensities.

In addition to the coherence change detection, differences in backscattering were investigated for the test site using all TSX images. An accurate co-registration of the scene of each stack to a single master was performed by employing a combination of the cross-correlation algorithm and iteratively refined look-up tables (generated based on the multilook intensity). We selected the image acquired on 4th December as the master and the coregistration process of the slave to the master resulted in precision of less than 0.1 pixels in the radar geometry. This guarantees that any product derived

from the scene will not affected by errors due to their relative co-registration. An optimum weighting filter namely De Grandi multitemporal speckle filter used to balance differences in reflectivity between images at different time was applied over TerraSAR-X time series. The local mean of backscatter coefficient has estimated from the data by averaging intensities values in a local window around each pixel in each image. During the geocoding procedure, the geometry of the scene has corrected using a 1arcsec DEM as input for converting the position of the backscattered elements into ground range image coordinates. The images were transformed by resampling to 5m spatial resolution using geographic coordinates on WGS84. Figure 4 shows an RGB false colour composite of backscatter temporal variability. The difference in radar response is given by changes in vegetation structure, ground surface roughness or dielectric constant of the soil which is function of the surface soil moisture. Trees and other vegetation are moderately rough and therefore they appear as height features with moderate backscattered intensity. When the rough surface becomes wet (TSX data acquired in December) the return signal increases due to a higher dielectric constant.

The multitemporal behaviour of backscatter coefficient has presented in figure 5. Forest stands dominated by the volume scattering effects show some signal dynamics through time whose peak values coincide with the period of minimum and maximum vegetative growth. The salt area shows small variations in time while the agricultural fields have characterized by phonological stage of crops, biomass and plant water content. Regarding multi-temporal behaviour of some probes, the 354 sample (that has affected by rapid land deformation) presents dynamic range of backscatter coefficients with the minimum and maximum associated with water inflow into the caverns. Other probes with a quite stable subsidence present small temporal variation.

The change detection by image differencing method (based on a cell-by-cell subtraction between different images in a time series) was performing on TSX intensity data to estimate vegetation coverage changes. Value of the thresholding level was calculeted by appling Otsu algorithm based on discriminant analysis and using zero and first order cumulative moments (Otsu, 1979). As is seen in Fig. 6, this method confirms previous results: the backscaterring changes are observed both in vegetated areas and in man-made structure.

Table1. Interferogram image pairs characteristics

Image pair	Perpendicular Baseline (m)	Height ambiguity (m)	Temporal baseline (days)
05.08.2010 04.12.2010	-75.12	75.387	121
04.12.2010 –03.08.2011	-85.78	66.077	242
05.08.2010 –03.08.2011	-159.4	35.529	363

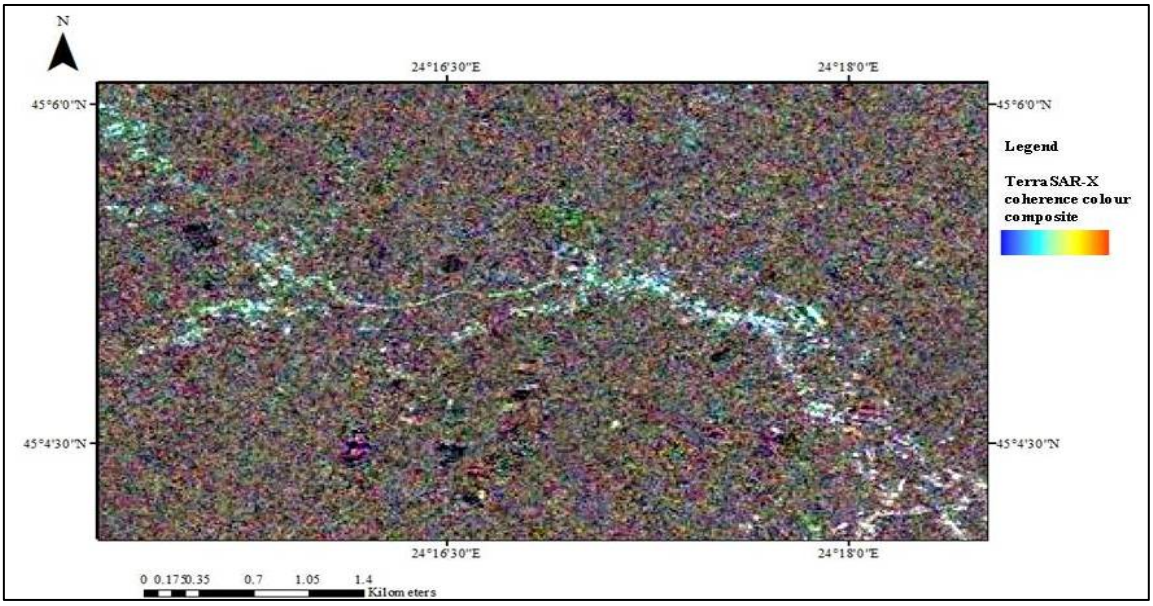

Figure 2. RGB false colour composite of coherence where R: first interferometric pair; G: second interferometric pair; B: third interferometric pair.

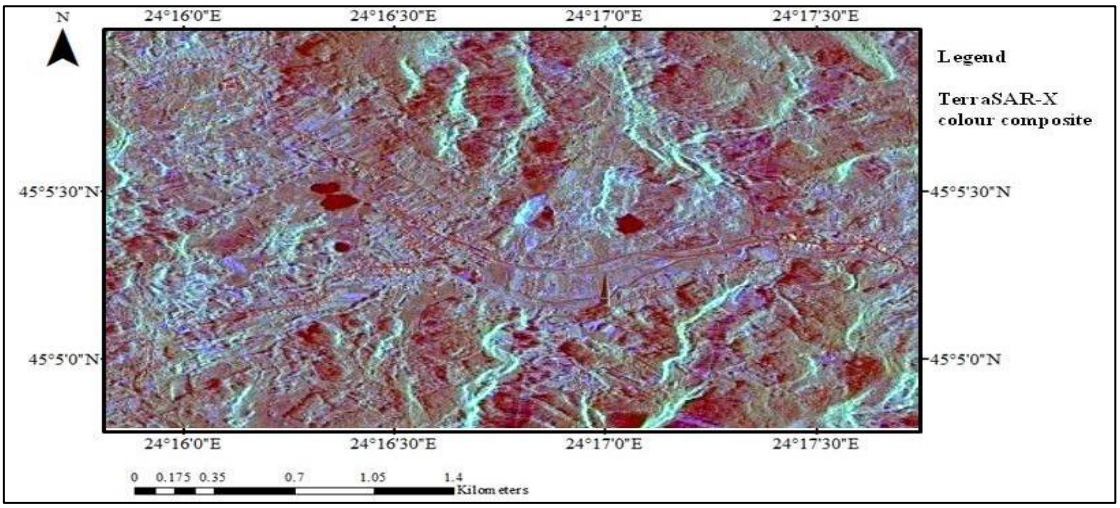

Figure 3. RGB false colour composite: R- coherence; G - 5.08.2010 intensity; B – 03.08.2011 intensity. The coherence has a lower value so that we observed seasonal changes in the forested and agricultural area.

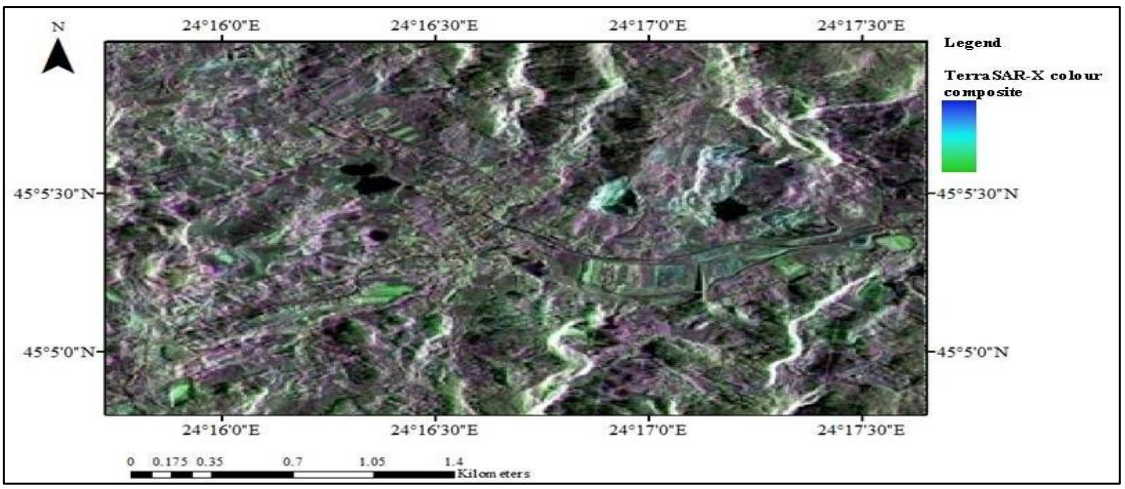

Figure 4. RGB false colour composite of intensities; green colour: decrease of backscatter values; white colour: foreshortening SAR effects, cyan colour: unchanged areas and purple: increase of backscatter values.

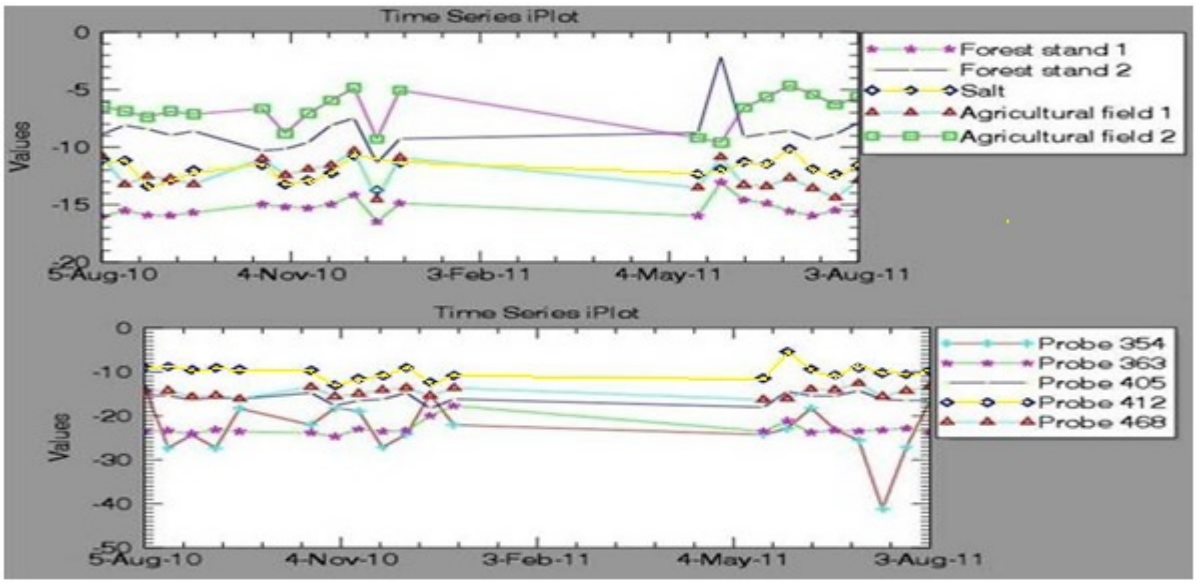

Figure 5. Temporal profiles of the backscatter coefficients. Bottom up: temporal evolution on land use/ land cover. Bottom down: temporal evolution of the some probes.

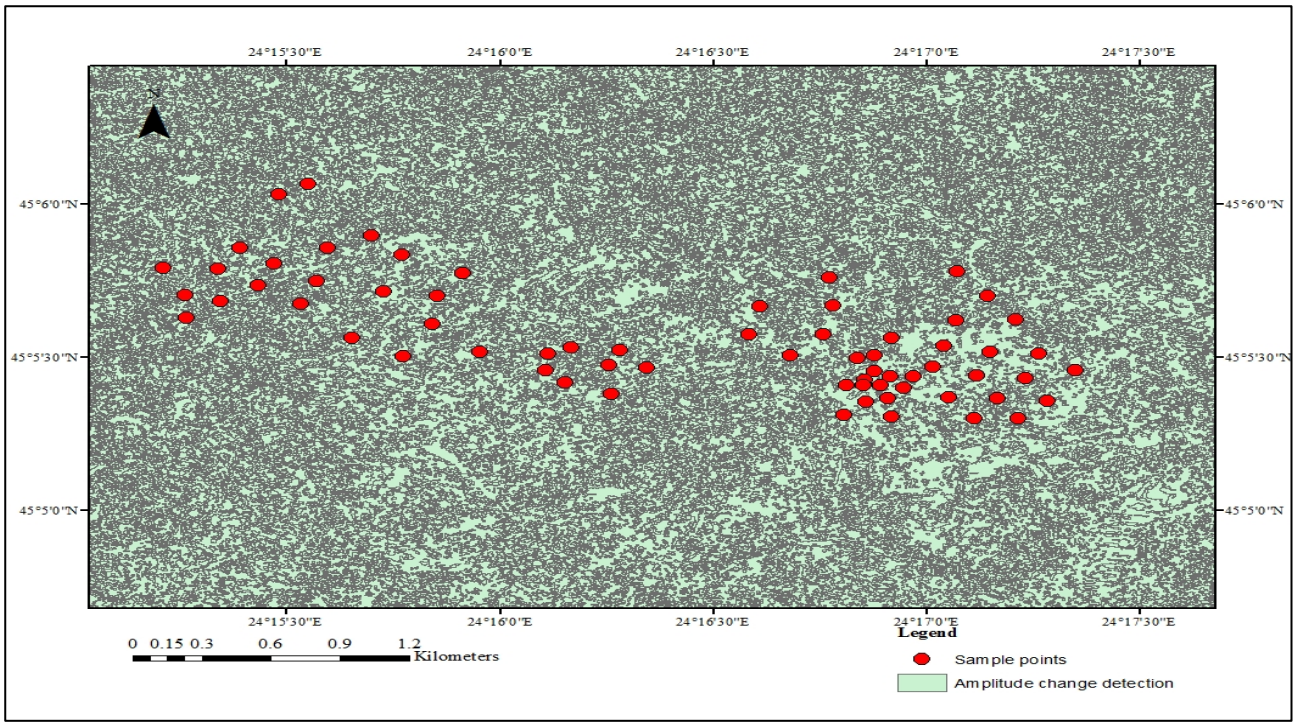

Figure 6. Amplitude change detection differences

3.3 Results for PSInSAR analysis

The InSAR PSI processing performed in Sarscape begins with the co-registration of all slave scenes in the interferometric stack to the master reference scene. The master image was chosen the image acquired on 4th December 2010 as it is less affected by the presence of vegetation. Using a Digital Elevation Model the interferogram stack is generated. Interferograms are flattened to the DEM and projected onto the master scene in slant range geometry. Goldstein adaptive filtering was applied to the interferogram to reduce noise introduced by decorelation and to improve the fringe signal-to-noise ratio. The coherence is then calculated. Next step is phase unwrapping. Unwrapping errors may occur in regions with low coherence especially in vegetated areas. The atmospheric pattern estimation is last processing step. The signal propagation through the troposphere can introduce delay in scatterer radar waves due to spatial and temporal variations in the water vapour content. Finally, a coherence threshold set to 0.3 is applied to the PS output data. We increased the PS number to 20000 in order to cover the salt mining area Ocnele Mari. The mean intensity and long-term coherence are shown in figure 7. The deformation velocity of PSs in line-of-sight is plotted in figure 8. In fact, most of the points show reduced or no deformation during the whole time span. a We observed small deformation (about of -2, - 4 mm/yr subsidence values) for the study are corresponding to the leveling measurements.

3.4 Results for PolInSAR analysis

Sentinel-1 dual polarized data acquired in configuration presented in table 2 were processed with Sentinel-1 toolbox. 3 X 3 Gamma Map and 7 X 7 median filters were applied on the S-1 data to reduce speckle noise. As is seen in figure 9, a RGB false colour composite, there are small variation in VV channel of the backscatter intensities between acquisitions (purple colour) while the green colour indicates a dominant VH component generally characteristic of vegetated area.

Terrain topography minimizes visual interpretation. We applied the Grey Level Coocurrence Matrix (GLCM) method to extract second order statistical texture features (Mohanaiah et al., 2013). This method is sensitive to the size of the texture samples on which they are estimated.

Table 2. Sentinel-1 data characteristics

Acquisition date	Imaging mode	Orbit	Polarization	Ground Range Resolution (m)
08.08.2014	IW, GRD	Ascending	VV+VH	10
20.08.2014	IW, GRD	Ascending	VV+VH	10

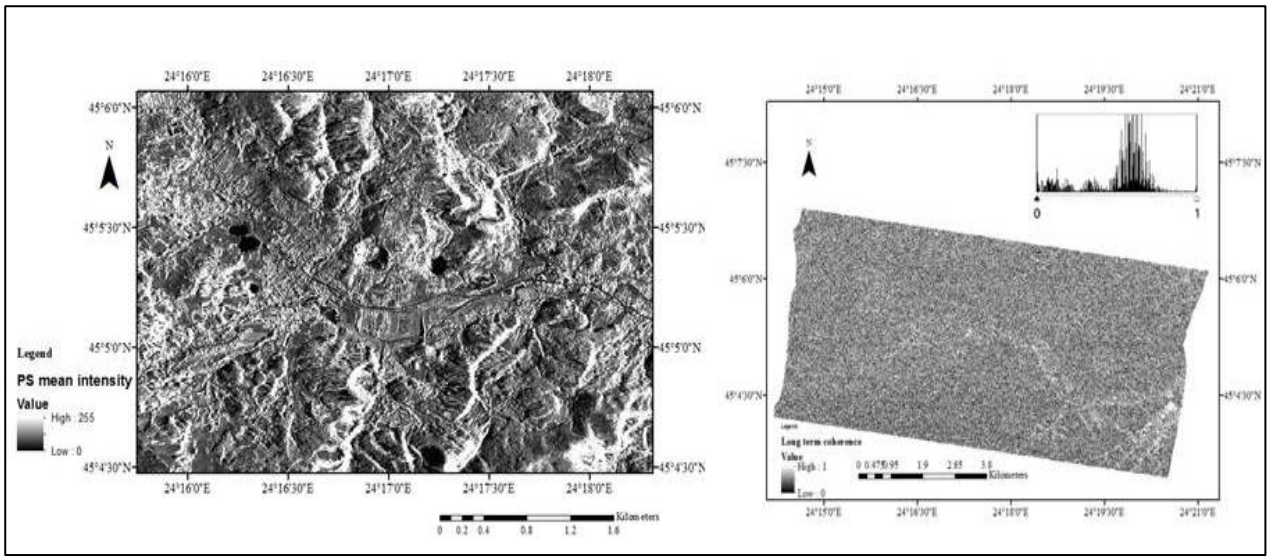

Figure 7. Mean intensity of the PSInSAR analysis, its long term coherence and the histogram.

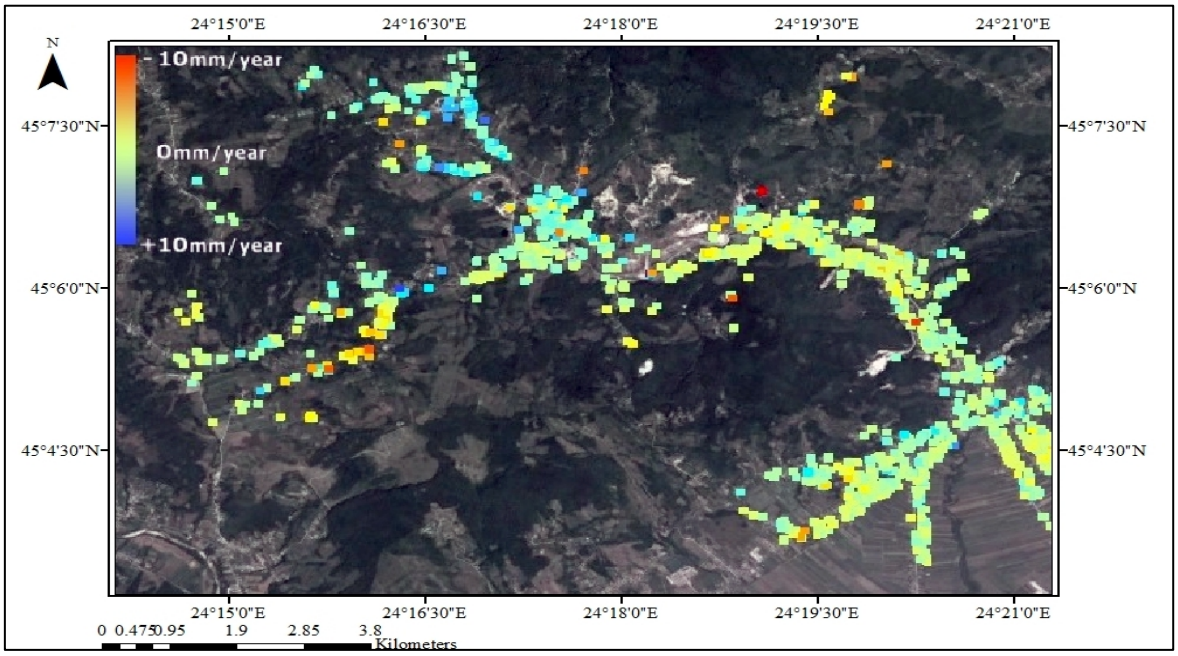

Figure 8. Deformation estimation with PSInSAR method: 20 TerraSAR-X Spotlight images were used. Acquisition on 4th December is master image. Estimated deformation velocity was coded with red-yellow-blue from -10 to +10 mm/year.

The texture analysis result is shown in figure 10: homogeneity is high in areas affected by layover; entropy is low due to loss of information in the SAR geometry, while correlation, which measures the linear dependency of grey levels of neighboring pixels, is higher. The unsupervised classification gave no results in this study.

Other C-band SAR data set acquired in June-September period by RADARSAT-2 sensor is used in this study to estimate the forest height. During this campaign, four SAR complex dual polarized (VV+VH) images, in ascending node, with effective baselines (perpendicular to the line-of-sight) ranging from -107 to -2 have been acquired (Table 3). The datawere processed with a single look of 5 m in range and 5 m in azimuth (100 MHz bandwidth). Figure 11 shows the slant range image of backscattered intensities, interferometric coherence and interferometric phase after flat earth removal. In the backscatter image the forest has the comparably strong and homogeneous radar backscatter intensity (-10 dB).

Streets and transition areas with shrubs are distinguishable. The coherence over the volume scatterer is lower than over double bounce scatters like roads and man-made structures. Over forests, the interferometric phase is more variable than other surfaces because the scattering centres are distributed randomly in the volume (Fig. 12).

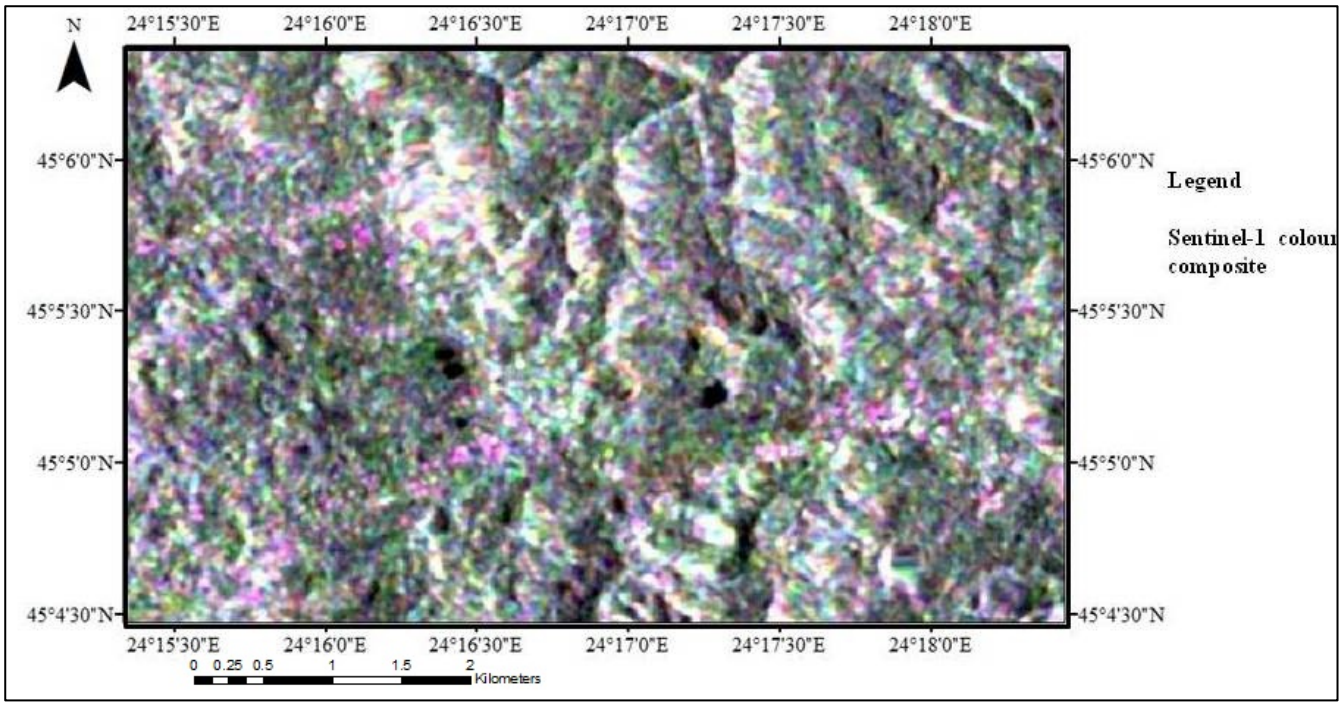

Figure 9. RGB false color composite: R- 08.08.2014 VV channel; G - 08.08.2014 VH channel; B – 20.08.2014 VV channel (© ESA)

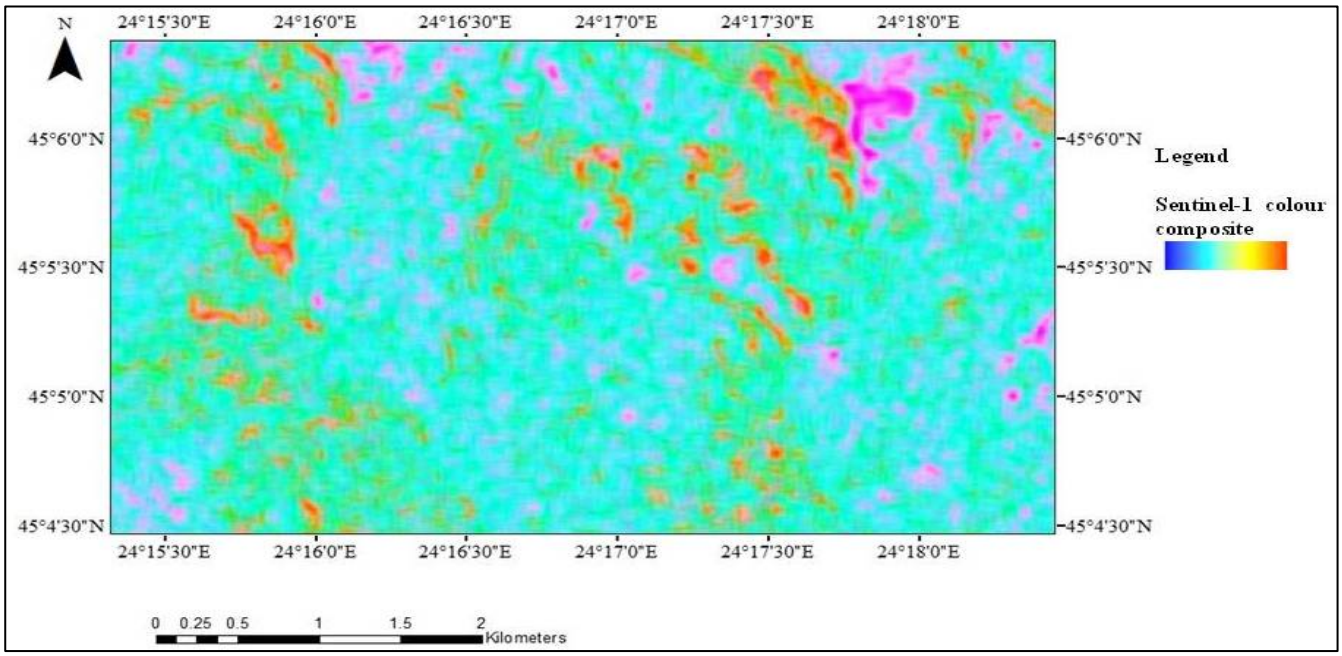

Figure 10. RGB false colour composit applied on S-1 data acquired in 8th August 2014: R- homogeneity; G – entropy, B – correlation.

Table3. Radarsat-2 interferogram image pairs characteristics

Image pair	Perpendicular baseline (m)	Height ambiguity (m)	Temporal baseline (days)
02.07-26.07.2014	-2.957	5457.201	24
26.07-19.08.2014	-107.423	150.213	24
19.08.12.09.2014	-90.623	178.061	24

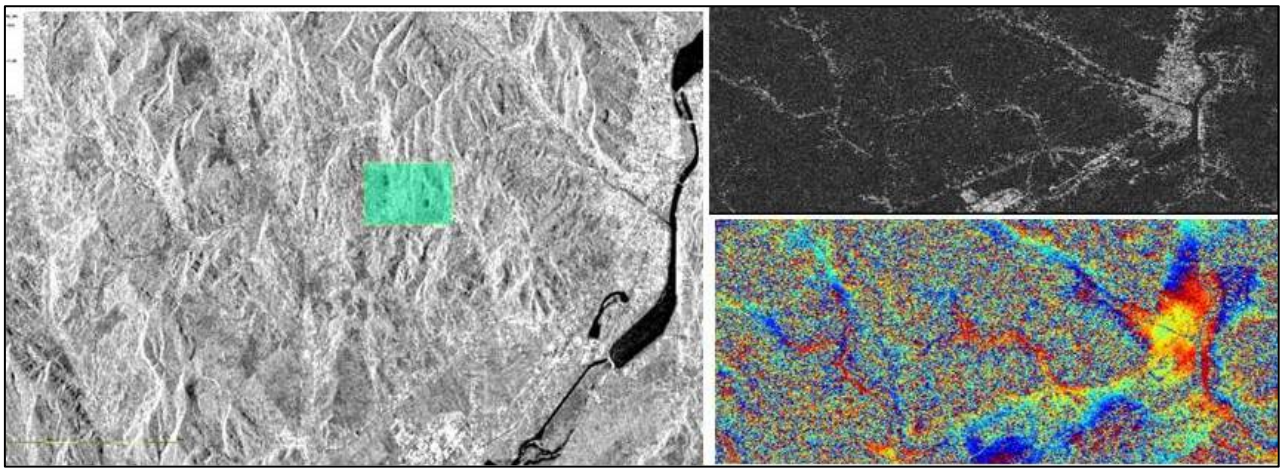

Figure 11. RADARSAT-2 data of the Ocnele Mari test site (VV polarization) (*RADARSAT-2 Data and Products© MacDonald, Dettwiler and Associates LTD (2014)- All right reserved. RADARSAT is an official trademark of the Canadian Space Agency):* Preliminary results: Backscatter intensity; interferometric coherence and interferometric phase after flat earth removal. The green square from intensity image represents Ocnele Mari salt mining area.

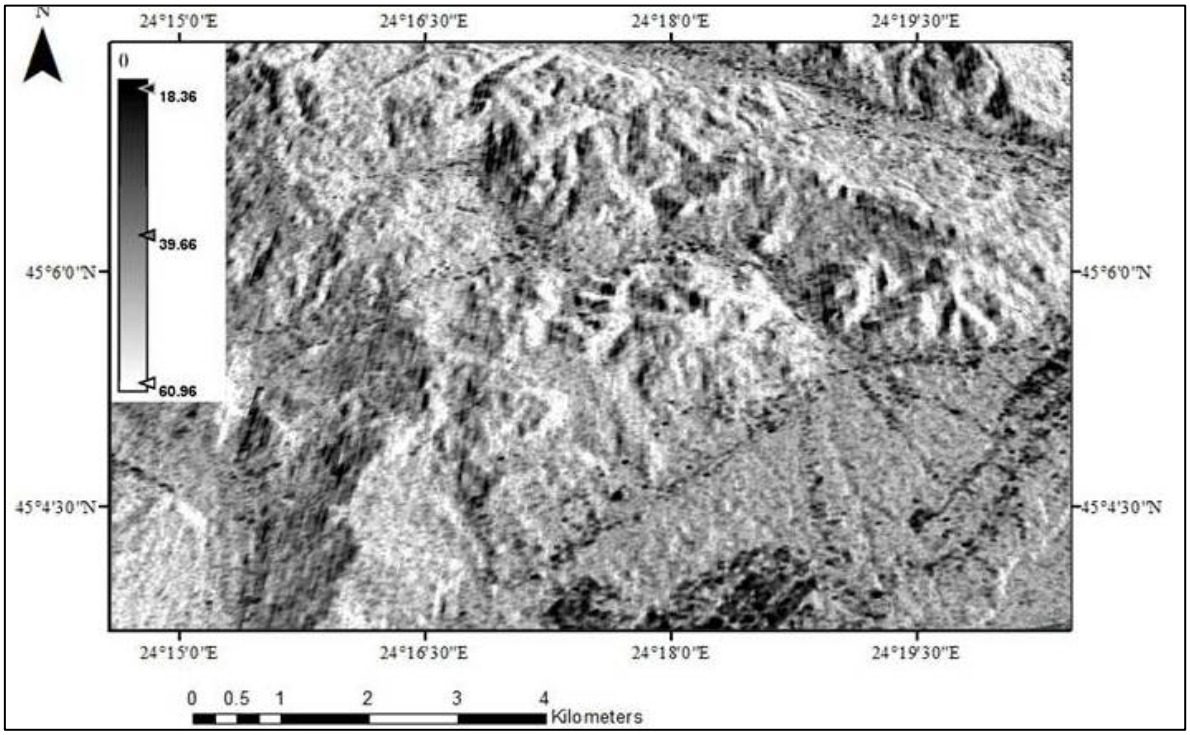

Figure 13. Sinc height inversion estimated from the second interferometric pair (-107m perpendicular baseline) (*RADARSAT-2 Data and Products © MacDonald, Dettwiler and Associates LTD (2014)- All right reserved. RADARSAT is an official trademark of the Canadian Space Agency)*

The sinc inversion assumes a constant temporal change and forest backscatter profile in height and does not take into consideration extinction and ground contribution. The relation only depends on height and vertical wavenumber k_z extracted from local incidence angle and is inverted from the coherence of VV component. Using a look-up table, the height is determined numerically (eq. 7).

$$h = 2 * sinc^{-1}(\gamma_{vol})/k_z \qquad (7)$$

The results are presented in figure 13. The extracted heights vary between 18 and 60 m whereby heights above 50 m occur more frequently in far range. It knows that VV channel is sensitive to vertical structures and provides good contrast among vegetation type with different vertical canopy structure. Therefore, to increase coherence, Radarsat-2 image was subset to an extended area of the Ocnele Mari test site.

The estimated height values above 18 m represented in black in the bottom of the image

correspond to the Oltchim chemical plant. Thus, this estimation cannot discriminate the height double bounce scatterering (ground contribution) of volume scattered so that is assigned to the minimum value. Maximum values are associated with layover. Erroneous low coherences generate overestimation of forest height. It shall be noted that the volume decorelation is not considered. We observed that HV dominates the volume coherence in the broadleaf stand whereas VV posses more ground contribution. These results cannot be validated due to absence of in-situ measurements. The ground bias will be resolved further in other study from the full RVoG inversion by choosing the polarization of the minimum ground contribution as γ_{vol}.

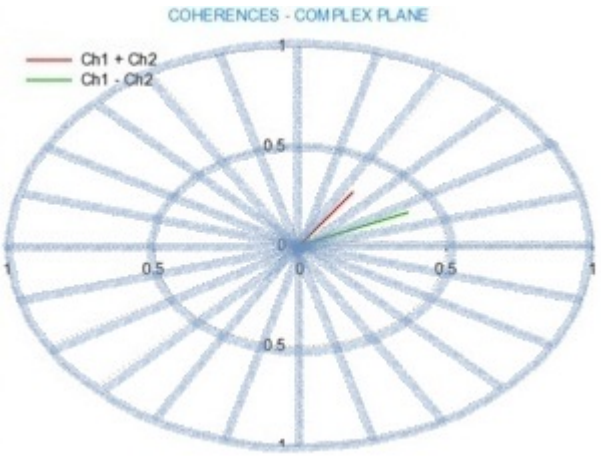

Figure 12. Forest coherence in complex plan

4. CONCLUSIONS

The study assessed the environment monitoring using SAR techniques with emphasis on temporal requirements and associated accuracy of outputs such as vegetation coverage and land degradation estimations in the Ocnele Mari salt mining area.

InSAR techniques are investigated for environment monitoring. The use of coherence change detection clearly shows that land changes can be observed in urban, non-vegetated areas. A general limitation of this method is the presence of vegetation which leads to decorrelation even for 11 days interferograms. The amplitude change detection is less sensitive to subtle changes, but it is much more robust and still provides valuable information. The combined use of coherence change detection with the amplitude change detection techniques offers a more complete picture of any changes observed.

PSInSAR technique is applied to estimate the land deformations using VHR Spotlight TerraSAR-X data. The PSInSAR is more appropriate and most suitable for the study of specific area / environment due to main advantages: filtering out of the atmospheric effects and elimination of the temporal and geometrical deccorelation. The results confirm the leveling measurements: after 2009 (when rehabilitation measures were been made in the Ocnele Mari salting area), a decreasing trend in subsidence rate (about few millimeter/year) is observed.

The PolInSAR technique is applied to estimate the forest height using C-band RADARSAT-2 fine Dual-Pol imagery (5 m ground resolution). The extracted heights are overestimated (varying between 18 m and 60 m). These results cannot be validated due to absence of in-situ measurements. Further studies will focuses on random volume of the ground inversion to solve ground bias and to improve estimation accuracy.

Acknowledgements

TerraSAR-X image data were acquired within the TerraSAR-X proposal LAN0778 submitted to DLR in 2010 by the Romanian Space Agency. Sentinel-1 data were acquired in the commissioning phase. Radarsat-2 imagery were acquired in the joint ESA-CSA SOAR Europe-16605 scientific proposal framework. The paper was done under the frame of European Social Fund, Human Resources Development Operational Programme 2007 -2013, project no POSDRU/159/1.5/S/132765.

REFERENCES

Aghababaee, H., Amini, J. & Tzeng, Y.C., 2013. *Improving Change Detection Methods of SAR Images Using Fractals*, Scientia Iranica A, 20(1), 15-22.

Bălteanu, D., Enciu, P. & Deak, G., 2006. *A large scale collapse in the Ocnele Mari salt mine field, Getic Subcarpathians, Romania*, Studia Geomorfologica Carpatho – Balcanica, XL, 119 – 126.

Bălteanu, D., 2000. *Present-day geomorphological processs and environmental change in the Romanian Carpathians*, Geomorphology of the Carpato-Balkan Region Conference, Romania, October 11-17, pp 123-128.

Bamler, R. & Hartl, P., 1998. *Synthetic aperture radar interferometry*, Inverse Problems, 14, R1-R54.

Cloude S.R. & Pottier E., 1996. *A Review of Target Decomposition Theorems in Radar Polarimetry*, IEEE Transactions on Geoscience and Remote Sensing, Vol. 34 No. 2, pp 498-518.

Cloude, S.R. & Papathanassiou, K.P., 1998. *Polarimetric SAR Interferometry*, IEEE Transactions on Geoscience and Remote Sensing, Vol. GRS-36. No. 5, pp. 1551-1565.

Cloude, S.R. & Papathanassiou, K.P., 2002. *A 3-Stage Inversion Process for Polarimetric SAR*

Interferometry, Proceedings of European Conference on Synthetic Aperture Radar, EUSAR'02, pp. 279-282, Cologne, Germany, 4-6 June 2002.

Cloude, S.R. & Papathanassiou, K.P., 2003. *A 3-Stage Inversion Process for Polarimetric SAR Interferometry*, IEE Proceedings, Radar, Sonar and Navigation, Volume 150, Issue 03, pp 125- 134.

Cumming, I. G. & Wong, **F. H.,** 2005. *Digital Processing of Synthetic Aperture Radar Data: Algorithms and Implementation*, Artech House, Boston.

Ferretti, A., Monti-Guarnieri, A., Prati, C., Rocca, F. & Massonnet, D., 2007. *InSAR Principles: Guidelines for SAR Interferometry Processing and Interpretation*, ESA Publications, The Netherlands, pp. A-7, A-8, A-17 – A-29, B-3, B-7 – B-30, B-31 – B-38, B-42 – B-49, C-56 – C-59, C-111.

Ferretti, A., Prati C. & Rocca F., 2000. *Nonlinear subsidence rate estimation using the Permanent Scatterers in differential SAR interferometry*. IEEE Transactions on Geoscience and Remote Sensing, 38(5), 2202-2012.

Ferretti, A., Prati C. & Rocca F., 2001. *Permanent scatterers in SAR interferometry*. IEEE Transactions on Geoscience and Remote Sensing, 39(1), 8-20.

Fomena, R.T. & Cloude, S.N., 2005. *On the Role of Coherence Optimization in Polarimetric SAR Interferometry*. In International CEOS SAR CAL/VAL workshop, Adelaide, Australia, September 2005.

Goldstein, R. M., Zebker, H. A., & Werner, C. L, 1988. *Satellite radar interferometry: Two-dimensional phase unwrapping*. Radio Sci., 23, 713–720.

Hooper, A., Segall, P. & Zebker, H., 2007. *Persistent scatterer interferometric synthetic aperture radar for crustal deformation analysis, with application to Volcán Alcedo, Galápagos*, Journal of Geophysical Research, Vol. 112, Issue B7.

Jiang, L., Liao, M., Zhang, L. & Lin, H., 2007. *Unsupervised change detection in multitemporal SAR images using MRF models*, Geo-spatial Information Science, Vol 10, issue 2.

Lavalle, M., Solimini, D., Pottier, E. & Desnos, Y.-L., 2007. *Comparasion of models of PolInSAR coherence for forest height retrieval using PolInSAR simulated data*, In Proc. Of Fringe Workshop, Frascati, Italy.

Lee, J.S., MR Grunes, M.R., Schuler, D.L., Pottier, E., 2006. *Scattering-model-based speckle filtering of polarimetric SAR data*, IEEE Transactions on Geoscience and Remote Sensing, 44, 176-187.

Licciardi, G.; Avezzano, R.G.; Del Frate, F.; Schiavon, G. & Chanussot, J., 2012. *Polarimetric sar target decomposition based on nonlinear decorrelation, Advances* in Radar and Remote Sensing (TyWRRS), 2012 Tyrrhenian Workshop on, vol., no., pp.283,287, 12-14 Sept. 2012.

Lu, H., Suo, Z., Guo, R. & ; Bao., Z., 2013. *S-RVoG model for forest parameters inversion over underlying topography*, Electronics Letters , vol.49, no.9, pp.618,620.

Luo, H.M.,; Chen, E.; Cheng; J. & Li, X., 2010. *Tree height retrieval methods using POLInSAR coherence optimization*, Geoscience and Remote Sensing Symposium (IGARSS), IEEE International, vol., no., pp.3259,3262.

Mocuta, M., Zamfirescu, F., Danchiv, A., Constantinescu, T. & Andrei, **M**., 2010. *Technical solution and monitoring results of the controlled collaps of Field 1 calt cavern, Ocnele Mari, Romania*, Solution Mining Research Institute, Tech. Meeting , Leipzing, Germany, 1-10.

Mohanaiah, P., Sathyanarayana, P. & GuruKumar, L., 2013 *Image Texture Feature Extraction Using GLCM Approach*, International Journal of Scientific and Research Publications, Volume 3, Issue 5.

Otsu, N., 1979. *A threshold selection method from gray level histograms*. IEEE Trans. Syst. Man Cybernet., 9: 62-66.

Poenaru, V.D., Badea, A., Savin, E., Teleaga, D. & Poncos, V., 2011. *Land degradation monitoring in the Ocnele Mari salt mining area using satellite imagery***,** Proceeding SPIE vol. 8181 818110U-1.

Pottier, E., Lee, J. S. & Ferro-Famil, L., 2004. *Advanced concept in polarimetry*, RTO Set Lecture series on "Radar Polarimetry and Interferometry.

Preiss, M., Grey, D.A. & Stacy, N.J.S., 2006. *Detecting scene changes using synthetic aperture radar interferometry*, IEEE Transactions on Geoscience and Remote Sensing, 44(8): 2041–2054.

Singh Ashbindu, 1989. *Review Article Digital change detection techniques using remotely-sensed data*, International Journal of Remote Sensing, 10:6, 989-1003.

Treuhaft, R.N. & Siqueira, P., 2000. *Vertical structure of vegetated land surfaces from interferometric and polarimetric radar*. Radio Sci, 35: 141–177.

Wang, H., Allain, S., Meric, S. & Pottier, E., 2013. *Scattering mechanism analysis using multi-angular polarimetric RADARSAT-2 datasets*, 6th International Workshop and Science and Applications of SAR Polarimetry and Polarimetric Interferometry, ESA Symposium, Jan 2013, Frascati, Italy. pp.1-6.

Xiong, B., Chen, Q., Jiang, Y. & Kuang, G., 2012. *A threshold selection method using two SAR change detection measures based on the Markov random field model*, IEEE Geos. Remote Sens. Lett., 9, pp. 287–291.

Zebker, H. A. & Goldstein, R. M.,1986. *Topographic mapping from interferometric synthetic aperture radar observations.* J. Geophys. Res., 91(B5), 4993–5000.

Zhang, L., Ding, X.L., & Lu, Z., 2011. *Modeling PSInSAR time series without phase unwrapping*. IEEE Transactions on Geoscience and Remote Sensing, 49, 547-556.

Received at: 17. 11. 2014
Revised at: 12. 03. 2015
Accepted for publication at: 29. 03. 2015
Published online at: 20. 04. 2015